AEI-2003-006
NSF-KITP-03-55

A numerical relativistic model of a massive particle in orbit near a Schwarzschild black hole

Nigel T. Bishop,[1] Roberto Gómez,[2,3] Sascha Husa,[4] Luis Lehner,[5,6] and Jeffrey Winicour[4,3]

[1] *Department of Mathematics, Applied Mathematics and Astronomy, University of South Africa, P.O. Box 392, Pretoria 0003, South Africa*
[2] *Pittsburgh Supercomputing Center, 4400 Fifth Ave., Pittsburgh, PA 15213, U.S.A.*
[3] *Department of Physics and Astronomy, University of Pittsburgh, Pittsburgh, PA 15260, U.S.A.*
[4] *Max-Planck-Institut für Gravitationsphysik, Albert-Einstein-Institut, Am Mühlenberg 1, D-14476, Golm, Germany*
[5] *Department of Physics and Astronomy, Louisiana State University, Baton Rouge, LA 70810, U.S.A.*
[6] *University of British Columbia, Vancouver, BC, Canada V6T-1Z1*

(Dated: September 10, 2003)

We present a method for computing the evolution of a spacetime containing a massive particle and a black hole. The essential idea is that the gravitational field is evolved using full numerical relativity, with the particle generating a non-zero source term in the Einstein equations. The matter fields are not evolved by hydrodynamic equations. Instead the particle is treated as a quasi-rigid body whose center follows a geodesic. The necessary theoretical framework is developed and then implemented in a computer code that uses the null-cone, or characteristic, formulation of numerical relativity. The performance of the code is illustrated in test runs, including a complete orbit (near $r = 9M$) of a Schwarzschild black hole.

PACS numbers: 04.25.Dm, 04.20.Ex, 04.30.Db, 95.30.Lz

arXiv:gr-qc/0301060v2 15 Sep 2003

I. INTRODUCTION

This paper is concerned with the evolution of a spacetime containing a small object in orbit near a black hole, the goal being to compute the motion of the object and the emitted gravitational radiation. In the techniques normally used for this type of 'radiation-reaction' problems, the small object is treated as a point-particle evolving on a fixed background spacetime with its self-force taken into account. There are a number of approaches concerning the implementation of the self-force – for example [1, 2, 3, 4, 5, 6, 7, 8, 9, 10, 11, 12]. An alternative approach that could be used is full numerical relativity including computational relativistic hydrodynamics (see for example [13, 14, 15, 16, 17, 18], and for a review [19]). To our knowledge, such simulations have not been performed for the extreme mass ratios considered in this paper.

The approach developed here uses full numerical relativity but with the hydrodynamic aspect greatly simplified, and can be described as a *polytropic particle (PP) method*. We use full numerical relativity for the evolution of the gravitational field (including a non-zero stress energy tensor as source). The matter fields are not evolved by relativistic hydrodynamics but rather the object is treated as a quasi-rigid body whose center is evolved by the geodesic equation. This approach avoids the intricacies and computational expense of relativistic hydrodynamics.

Of course, there are limitations to the PP approach: it can only be applied in situations in which the internal hydrodynamics of the material object are unimportant, and in which the rigidity approximation is reasonable. For example, one would certainly need full numerical relativity and relativistic hydrodynamics in situations in which the object is expected to be tidally disrupted. On the other hand, if tidal effects are small (in a sense that will be made precise), then the PP model should provide a good description of the physics.

The bounds of the domain of applicability of the PP method have not been investigated systematically. However, from the example runs presented in Sec. V, the method should be applicable under appropriate restrictions, e.g. when $m \leq 10^{-5}M$ where M is the mass of the black hole and m is the mass of the particle, and when the size of the particle is small enough that it not be tidally disrupted. Thus, we expect the particle method to be applicable in astrophysical situations involving the inspiral and capture of a neutron star or white dwarf by a galactic black hole (with M about $10^6 M_\odot$). On the other hand, it is difficult to see how the method could be used for a stellar remnant black hole (with M about $10M_\odot$) – any object with small enough m/M would have too large a diameter. Thus the method is expected to make predictions concerning gravitational radiation that will be relevant to observations by LISA [20], rather than to observations by LIGO or other earth based detectors.

The results presented here use a characteristic gravity code [21, 22]. However, there is no reason to restrict the PP method to the characteristic approach. The method should also be applicable within Cauchy formulations of numerical relativity.

We have also constructed a finite difference version of a $\delta-$function model. We found that the PP model performs better, giving smoother results and, in particular, exhibiting convergence with grid-refinement (as described in Sec. V A). For these reasons, although we describe both models, we give implementation details and results only for the PP model.

The purpose of this paper is to introduce the PP

method. We also give some example runs exhibiting inspiral and a plunge to the black hole. These runs demonstrate the potential of the method, and are not an accurate description of the physics – in particular, in the inspiral case, the inspiral rate is much larger than that predicted by other methods. Of course, validated physical results are the goal of this project but, as discussed in Sec. VI, more computational testing and development is needed before the goal can be attained.

We begin by summarizing previous results on the characteristic formulation of numerical relativity in Sec. II. Issues concerning the theoretical framework of a massive particle are discussed in Sec. III. Sec. IV presents, in detail, the computational algorithms. Tests of the code and example runs are given in Sec. V.

II. SUMMARY OF PREVIOUS RESULTS, AND NOTATION

The formalism for the numerical evolution of Einstein's equations, in null cone coordinates, is well known [21, 23, 24] (see also [25, 26, 27, 28, 29]). For the sake of completeness, we give here a summary of the formalism, including some of the necessary equations. The version of the gravity code being used here is fully described in [22].

We use coordinates based upon a family of outgoing null hypersurfaces. We let u label these hypersurfaces, x^A ($A = 2, 3$), label the null rays and r be a surface area coordinate. In the resulting $x^\alpha = (u, r, x^A)$ coordinates, the metric takes the Bondi-Sachs form [28, 30]

$$\begin{aligned} ds^2 &= -\left(e^{2\beta}(1+\frac{W}{r}) - r^2 h_{AB}U^A U^B\right) du^2 - 2e^{2\beta} du dr \\ &\quad - 2r^2 h_{AB} U^B du dx^A + r^2 h_{AB} dx^A dx^B, \end{aligned} \tag{2.1}$$

where $h^{AB}h_{BC} = \delta^A_C$ and $det(h_{AB}) = det(q_{AB})$, with q_{AB} a unit sphere metric. We work in stereographic coordinates $x^A = (q, p)$ for which the unit sphere metric is

$$q_{AB}dx^A dx^B = \frac{4}{F^2}(dq^2 + dp^2), \text{ where } F = 1 + q^2 + p^2. \tag{2.2}$$

(In previous notation we used $P = 1 + q^2 + p^2$. Here we change notation to F because P now represents pressure, which we cannot denote by p because that is a stereographic coordinate). We also introduce a complex dyad $q^A = \frac{F}{2}(1, i)$ with $i = \sqrt{-1}$. For an arbitrary Bondi-Sachs metric, h_{AB} can then be represented by its dyad component

$$J = h_{AB} q^A q^B/2, \tag{2.3}$$

with the spherically symmetric case characterized by $J = 0$. We introduce the (complex differential) eth operators $\eth$ and $\bar{\eth}$ (see [31] for full details), as well as a number of auxiliary variables $K = h_{AB}q^A\bar{q}^B/2$, $U = U^A q_A$, $Q_A = r^2 e^{-2\beta} h_{AB} U^B_{,r}$, $Q = Q_A q^A$, $B = \eth\beta$, $\nu = \bar{\eth}J$ and $k = \eth K$.

The Einstein equations decompose into hypersurface equations, evolution equations and conservation laws. The hypersurface equations form a hierarchical set for $\nu_{,r}$, $k_{,r}$, $\beta_{,r}$, $B_{,r}$, $(r^2Q)_{,r}$, $U_{,r}$ and $W_{,r}$; and the evolution equation is an expression for $(rJ)_{,ur}$. The explicit form of the equations is given in [22] in the vacuum case. The matter source terms, in the case of a perfect fluid of density ρ, pressure P and velocity v^α, are stated in [32]; except the matter source term in Eq. [32]–(31) is incorrect and that equation should read

$$\begin{aligned} &2\left(rJ\right)_{,ur} - \left(\left(1 + r^{-1}W\right)\left(rJ\right)_{,r}\right)_{,r} = -r^{-1}\left(r^2\eth U\right)_{,r} \\ &+2r^{-1}e^{\beta}\eth^2 e^{\beta} - \left(r^{-1}W\right)_{,r} J + N_J \\ &+\frac{4e^{2\beta}\pi(\rho + P)}{r}\left((J\bar{V}_{ang} - KV_{ang})^2 + V^2_{ang}\right), \end{aligned} \tag{2.4}$$

where $V_{ang} = v_A q^A$ [32], and N_J is defined in [21] and [22]. The remaining Einstein equations reduce to conservation conditions which need only be satisfied on the inner boundary, which are automatically satisfied here because the boundary has a simple Schwarzschild geometry.

The null cone problem is normally formulated in the region of spacetime between a timelike or null worldtube Γ and $\mathcal{I}^+$. We represent $\mathcal{I}^+$ on a finite grid by using a compactified radial coordinate $x = r/(1 + r)$. The numerical grid is regular in (x, q, p) and consists of two patches (north and south), each containing $n_x n_q n_p$ grid-points. The $x-$grid covers the range $[0.5, 1]$. Each angular grid patch extends two grid-points beyond the domain $(q, p) \in [-q_s, q_s] \times [-q_s, q_s]$, with $q_s \geq 1$. Thus there is an overlap region at the equator with larger overlap for larger q_s.

We denote the Bondi-Sachs metric (2.1) by $g_{\alpha\beta}$ and the background metric ($g_{\alpha\beta}$ with $J = U = \beta = 0$, $W = -2M/r$) by $g_{[M]\alpha\beta}$. The mass M of the black hole is normally scaled to $M = 1$ in simulations.

III. THEORETICAL FRAMEWORK

We have developed two different particle models with rather different conceptual frameworks but implemented with very similar numerical codes. This section describes each of the two frameworks, as well as some other theoretical issues.

A. The polytropic particle (PP) model

The PP model treats the particle as an object of fixed size in its local proper rest frame, with its center $z^\alpha(u)$ describing a geodesic of the full spacetime. The particle is treated as quasi-rigid, and a simple formula is used to evaluate the stress-energy tensor, which then appears as source in the Einstein equations. The simplest model of a polytrope, which will be used here, is for the case with

index $n = 1$. Then the density ρ and pressure P of an equilibrium configuration are given by [33]

$$\rho = \frac{m \sin \frac{R\pi}{R_*}}{4RR_*^2}, \quad P = \frac{2R_*^2\rho^2}{\pi}, \tag{3.1}$$

for $R \leq R_*$, and $\rho = P = 0$ for $R > R_*$, where R_* is the radius of the polytrope and R is the distance from its center.

The density $\rho(R)$ and pressure $P(r)$ at a point $x^\alpha = (u, x^i)$ in the Bondi-Sachs coordinate system are set by determining the distance R, in the local proper rest frame, between x^α and the geodesic described by the center of the polytrope. We first define the displacement vector ϵ^α relative to the polytrope's center,

$$\epsilon^u = 0, \quad \epsilon^i = x^i - z^i(u). \tag{3.2}$$

The projection of ϵ^α into the hypersurface orthogonal to the worldline at time u is

$$R_\alpha = (g_{\alpha\beta} + v_\alpha v_\beta)\epsilon^\beta, \tag{3.3}$$

with $g_{\alpha\beta}$ evaluated at z^α, and v_α evaluated at time u. Then we define the proper distance R as the magnitude of R_α,

$$R = \sqrt{g^{\alpha\beta}R_\alpha R_\beta}, \tag{3.4}$$

and set the density and pressure using Eq. (3.1). Thus, in its local proper rest frame, a (small) polytropic particle is a spherically symmetric object with proper radius R_*. The perfect fluid condition is used to set the stress-energy tensor, i.e. $T_{\alpha\beta} = (\rho + P)v_\alpha v_\beta + P g_{\alpha\beta}$.

The PP model is approximate in the following sense. Equation (3.1) is exact only for an isolated sphere in equilibrium in Newtonian theory. In general relativity it is a good approximation if $m \ll R_*$ (and the example runs presented later satisfy this condition). Further, in the field of a black hole, a polytrope would not preserve its spherical shape but would become tidally distorted. Both these approximations introduce the same type of error – the PP's motion is treated as quasi-rigid but, for the purpose of determining its gravitational field, its stress-energy tensor $T_{\alpha\beta}$ is modeled as a perfect fluid. Thus there are contributions to $T_{\alpha\beta}$ that are being ignored, and the magnitude of these contributions is now estimated.

Firstly, since the simulations in Sec. V satisfy the condition $m \ll R_*$, the error in ignoring the tidal stress will dominate that of using Eq. (3.1) to estimate the pressure. We use Newtonian theory to make an order of magnitude estimate of the tidal stress. The tidal acceleration in the radial direction is $2Mx/r^3$ where x is the distance from the center of the polytrope. The tidal stress is maximum at the center of the polytrope, and a simple dimensional argument (which can be confirmed by integration) shows that

$$\sigma_{\max} = \mathcal{O}\left(\frac{Mm}{r^3 R_*}\right). \tag{3.5}$$

In order to estimate the significance of $\sigma_{\max}$ in the stress-energy tensor, we compare it to the maximum density

$$\frac{\sigma_{\max}}{\rho_{\max}} \equiv S = \mathcal{O}\left(\frac{4R_*^2 M}{\pi r^3}\right). \tag{3.6}$$

In a physical situation in which the polytrope is stable against tidal disruption, $(MR_*^3)/(mr^3) < \mathcal{O}(1)$, and the ratio S is smaller than $\mathcal{O}(m/R_*)$, which, as previously noted, is small here. However, in the example to be considered in Sec. V B, the polytrope is not stable against tidal disruption, and thus the internal stresses may be large. In fact, the ratio S is approximately $4/(81\pi) \approx 0.016$.

B. The $\delta-$function model

At the analytic level, a point particle of mass m at position $z^\alpha = (u, z^i) = (u, r, z^A)$ has density ρ and 4-velocity v^α satisfying

$$\rho\sqrt{-g}v^u = m\delta(x^i - z^i), \tag{3.7}$$

where $\int \delta(x^i - z^i)drdqdp = 1$. We model the δ-function on the grid by assigning weights w to each grid point in a stencil surrounding the particle. In terms of a test function ϕ, this requires

$$\phi(z^i) = \Sigma_I \phi_I w_I \Delta_V \tag{3.8}$$

where Σ_I is a sum over a stencil I of grid points surrounding the particle position z^i and Δ_V is the coordinate 3-volume of the stencil I. We determine the weights w_I representing the δ-function by choosing a set of test functions, e.g. for the stencil of eight points determined by the cell surrounding the particle we choose

$$\begin{aligned} \phi &= a + a_i(x^i - z^i) + a_{ij}(x^i - z^i)(x^j - z^j) \\ &+ a_{ijk}(x^i - z^i)(x^j - z^j)(x^k - z^k), \end{aligned} \tag{3.9}$$

where $i \neq j \neq k$ so that the a's constitute eight arbitrary coefficients. This then gives 8 simultaneous equations to solve for the w_I, which are given explicitly in Eq. (4.6) below.

It is necessary to renormalize the metric so as to avoid infinities in the equations of motion. The metric occurs through the normalization of the 4-velocity v_α and the raising of indices. We take the components (v_r, v_A) to be basic since they represent the pullback of the 4-velocity to the null hypersurface. We renormalize the other components by using the background metric $g_{[M]\alpha\beta}$ to raise indices and to normalize the 4-velocity. This avoids the problem of an infinite self-potential energy of the particle and is in keeping with the principle that the energy of the particle only depends on its velocity and position in the Schwarzschild field. It should be emphasized that this renormalization, or use of $g_{[M]\alpha\beta}$ rather than $g_{\alpha\beta}$, applies only to the *undifferentiated* metric. Metric derivatives that occur in the particle equations of motion are

computed using the full metric $g_{\alpha\beta}$ – otherwise radiation reaction could not be included and we would simply be computing the motion of a test particle in the Schwarzschild geometry. Of course, it is the full metric which is evolved by the characteristic algorithm.

Although we were able to use the δ-function model to compute qualitatively reasonable orbits for the problems considered in Secs. V B and V C, they were significantly less smooth than with the PP model, and the growth in the deviation from a Schwarzschild orbit was much faster. Further, we did not find any quantity that exhibited convergence, making it problematic to use the δ-function model to obtain physical predictions. Perhaps a more sophisticated numerical approach might lead to convergence of global quantities, but this would be a difficult project that we do not pursue here.

C. Modeling the particle orbit

A goal of this work is to study radiation reaction. This is a small effect, and, numerically, it could be hidden if terms of order unity (representing the background Schwarzschild geometry) are added and subtracted in the equations of motion. The motion of a test particle in a background Schwarzschild geometry satisfies certain conservation laws; the motion of a particle with mass $0 < m \ll M$ does not satisfy these laws, but they are nevertheless useful because these laws indicate quantities that change very slowly. Our strategy is to use the Schwarzschild conservation laws to find quantities that, in the general case, evolve slowly. In the process, all background Schwarzschild terms cancel out and we are left with expressions involving only small quantities.

For the case of a test particle in the Schwarzschild geometry there is a reflection symmetry plane, the plane of the orbit. Thus the normalized 4-velocity is completely determined by its components $T^\alpha v_\alpha = v_u$ and $\Phi^\alpha v_\alpha = v_\phi$, where T^α and Φ^α are the Killing vectors of the Schwarzschild background and v_ϕ is a velocity component with respect to (u, r, θ, ϕ) null-spherical coordinates. In the general case, v_u and v_ϕ are approximately conserved. Partly because of the stereographic coordinates being used, the implementation is quite technical (see Sec. IV D for details).

D. Caustics

The characteristic evolution code breaks down if caustics develop, which render the null coordinate system employed singular. A rough estimate can be readily obtained by employing the well-known condition for the deflection of light by a massive body such as the Sun. We find as an approximate condition for caustics not to form that

$$\frac{R_*^2}{4m} > r. \tag{3.10}$$

IV. COMPUTATIONAL METHOD

A. Overview

The PP method evolves both the matter and gravity fields. At each grid-point at which the density is nonzero, the particle's density, pressure and 3-velocity are found and used to construct the right hand side of the Einstein equations, and the gravitational field is then evolved as described in Sec. II. The gravitational field affects the motion of the particle: the 3-velocity v_i is evolved by using the geodesic equation in the form

$$\frac{dv_i}{du} = \frac{\Gamma_{\alpha i\gamma} v_\delta v_\epsilon g^{\alpha\delta} g^{\gamma\epsilon}}{v^u}; \tag{4.1}$$

and the particle's position is evolved by

$$\frac{dz^i}{du} = \frac{v^i}{v^u}. \tag{4.2}$$

The setting of initial data is described in Sec. IV C below. The worldtube Γ at $r = 2M$ is the (past) horizon of a Schwarzschild black hole of mass M. Thus the boundary data on Γ has the simple analytic form [32]

$$J = \nu = k = \beta = B = U = Q = 0, \;\; W = -2M. \tag{4.3}$$

B. Computational algorithms

The iterative evolution algorithm proceeds as follows:

1. Start at time $u = u^{(n)}$. The gravitational field $g_{\alpha\beta}^{(n-1)}$ is known over the whole grid and the boundary data supplies $g_{\alpha\beta}^{(n)}$ in a neighborhood of $r = 2M$. The particle's position $z^{i(n)}$ and velocity $v_i^{(n)}$ are also known.

2. Determine the grid-cell $G_P^{(n)}$ containing the point $z^{i(n)}$; i.e., determine a_i such that

$$\begin{aligned} r^{(a_1)} < z^{1(n)} < r^{(a_1+1)}, \\ q^{(a_2)} < z^{2(n)} < q^{(a_2+1)}, \\ p^{(a_3)} < z^{3(n)} < p^{(a_3+1)}. \end{aligned} \tag{4.4}$$

This is done on both north and south patches, although if the particle is not in the equatorial overlap region there will be a solution for only one of the patches. We define

$$\Delta^{i(n)} = x^{a_i+1} - x^{a_i}, \qquad \delta_0^{i(n)} = x^{a_i+1} - z^{i(n)}, \qquad \delta_1^{i(n)} = z^{i(n)} - x^{a_i} \tag{4.5}$$

and we define weights at the eight grid-points at the corners of $G_P^{(n)}$ by

$$w(x^{a_i+e_i}) = \frac{\delta_{e_1}^{1(n)} \delta_{e_2}^{2(n)} \delta_{e_3}^{3(n)}}{\Delta^{1(n)} \Delta^{2(n)} \Delta^{3(n)}}, \tag{4.6}$$

where $e_i = \{0, 1\}$.

3. Next, we set the density and pressure. In general, this needs to be done on both north and south patches. The density at the grid-point x^i is set by means of Eqs. (3.1)-(3.4); then the pressure P is set.

4. The Einstein equations are now integrated to find the metric $g^{(n)}_{\alpha\beta}$. The source terms are given in [32] (where, as already noted, Eq. [32]-(31) should be replaced by Eq. (2.4)).

5. The formula $g^{\alpha\beta}v_\alpha v_\beta = -1$ is used to find $v^{(n)}_u$; the metric $g^{\alpha\beta}$ is known at the required grid-points and its value at the particle position $z^{i(n)}$ is found by taking a weighted average using the weights found in Eq. (4.6) above.

6. The formula $v^\alpha = g^{\alpha\beta}v_\beta$ is used to find $v^{\alpha(n)}$, again using the weighted average to find $g^{\alpha\beta}$.

7. Equation (4.2) is now used to find $z^{i(n+1)}$. On the first time-step, this is done by the Euler method and, on subsequent time steps, by the 3-point Adams-Bashforth method, i.e.

$$z^{(n+1)} = z^{(n)} + \frac{\Delta u}{2}\left(3\frac{dz}{du}^{(n)} - \frac{dz}{du}^{(n-1)}\right) \tag{4.7}$$

8. We now find $v_i^{(n+1)}$. The right hand side of Eq. (4.1) is evaluated at $z^{i(n)}$ by, as usual, finding the value at the grid-points and taking a weighted average using the weights found in Eq. (4.6) above. The terms in Eq. (4.1) are quite complicated and were found using a Maple script, which was also used to generate Fortran code. Details are given in an Appendix. The numerical evolution method is the same as used in step 7.

C. Setting the initial data

We have experimented with various ways of setting the initial data, and found that, apart from some early transient effects, the options tried make little difference to both the particle orbit and the gravitational field. The initial gravitational content is prescribed by setting $J = 0$ at $u = 0$. (It is also possible to set the initial data J by a Newtonian limit condition [23, 34, 35], the computational implementation of which will be discussed elsewhere). Of course, this means that we are introducing spurious gravitational radiation into the initial data, which might have the effect of initializing the particle into a different orbit to that intended. We tried evolving the code for a pre-determined time u_S (and u_S could be possibly set to zero), during which time the particle's velocity and position are not updated. The idea is that the gravitational field should relax to the correct form, with the spurious initial gravitation content radiating away, by the time u_S when the particle is allowed to move.

The code requires the initial velocity as a 1-form v_i but a physical description normally specifies the tangent vector v^i. For example, a particle in a circular orbit would have

$$v^r = 0, \;\; (v^p)^2 + (v^q)^2 = \frac{F^2 M}{4r^2(r-3M)}. \tag{4.8}$$

Suppose that we are given v^i rather than v_i. Initially, when only the background metric is known, v_i is constructed from v^i using

$$g_{[M]\alpha\beta}v^\alpha v^\beta = -1 \tag{4.9}$$

to first determine v^u; then $v_i = g_{[M]i\alpha}v^\alpha$. Then, while $u \le u_S$, the code uses the fact that v^α is found at each time step to determine a value of v_r such that $v^r = 0$ by an iterative algorithm. Explicitly, we use the secant algorithm

$$v_{r(a+1)} = v_{r(a)} - v^r_{(a)} f_S \frac{v_{r(a)} - v_{r(a-1)}}{v^r_{(a)} - v^r_{(a-1)}}, \tag{4.10}$$

where a is the iteration number and f_S is a factor (which is 1 in the standard algorithm) that may need to be set to 0.2 or smaller for stable convergence – the difficulty here is that we are solving $v^r(v_r) = 0$ not as a simple algebraic equation but as an equation whose coefficients change as the metric relaxes.

We found that the value of u_S has little effect on computed orbits, at least for the cases computed in Sec. V B below. Thus, we will set $u_S = 0$. Nevertheless, the option of setting a non-zero u_S is retained in the code in case circumstances are found in which a smoother evolution is obtained.

D. Implementation of the approximate conservation laws

The theoretical basis for using approximate angular momentum and energy conservation to improve the accuracy of the orbit computation, was discussed in Sec. III C. We now present details of how this is implemented for (1) the angular momentum in an equatorial orbit, (2) the angular momentum in a polar orbit, and (3) the energy. The code is written so that all of these approximate conservation laws may be used, or not, simply by changing input parameter switches.

1. Angular velocity in an equatorial orbit

The angular momentum per unit mass

$$h = qv_p - pv_q \tag{4.11}$$

is approximately conserved. In terms of proper time τ along the particle's trajectory,

$$\frac{dh}{d\tau} = v^q v_p + q\frac{dv_p}{d\tau} - v^p v_q - p\frac{dv_q}{d\tau}. \tag{4.12}$$

Now, Eq. (4.1) takes the form

$$\frac{d}{d\tau}v_A = -\frac{z^A}{r^2}\left((v_p)^2 + (v_q)^2\right) + E_A, \quad A = (q,p), \tag{4.13}$$

where the E_A contain only small quantities. We also introduce the small quantity $\mu^i = (g^{i\alpha} - g^{i\alpha}_{[M]})v_\alpha$, which represents the difference between raising an index of the covariant velocity by the full or background metric. Thus,

$$v^A = \mu^A + \frac{v_A}{r^2}. \tag{4.14}$$

Combining Eqs. (4.12), (4.13) and (4.14), we obtain

$$\frac{dh}{d\tau} = \mu^q v_p - \mu^p v_q + qE_p - pE_q, \tag{4.15}$$

which is implemented in the code. We extract v_A from the evolved value of h. This is done by using the constraint that the particle is on the equator, $q^2 + p^2 = 1$. Thus $qv^q + pv^p = 0$ so that

$$q\left(\mu^q + \frac{v_q}{r^2}\right) + p\left(\mu^p + \frac{v_p}{r^2}\right) = 0. \tag{4.16}$$

Combining Eqs. (4.11) and (4.16), we find

$$\begin{aligned} v_q &= -ph - r^2 q(q\mu^q + p\mu^p) \\ v_p &= qh - r^2 p(q\mu^q + p\mu^p), \end{aligned} \tag{4.17}$$

which is implemented in the code. Furthermore, the particle is constrained to follow the equator exactly, and so the particle's position is corrected according to $z^A \to z^A f_e$ with

$$f_e = \sqrt{\frac{1}{q^2 + p^2}}. \tag{4.18}$$

2. Angular velocity in a polar orbit

In the case of polar motion, simplified here to the case $p = 0$, the equations analogous to Eqs. (4.11), (4.15) and (4.17) are

$$h = \frac{Fv_q}{2}, \quad \frac{dh}{d\tau} = \frac{FA_q}{2} + qv_q\mu^q, \quad v_q = \frac{2h}{F}. \tag{4.19}$$

3. The energy

The energy per unit mass v_u is conserved along a geodesic in the Schwarzschild background. In this case

$$v_{uS} = \frac{h^2 + r^2 + v_r^2(r^2 - 2Mr)}{2v_r r^2}. \tag{4.20}$$

We take v_{uS}, as defined above, to be an approximately conserved quantity. From Eq. (4.1),

$$\frac{d}{d\tau}v_r = -\frac{h^2}{r^3} - \frac{v_r^2 M}{r^2} + E_1. \tag{4.21}$$

Using

$$\frac{dr}{d\tau} = v^r = -v_{uS} + \left(1 - \frac{2M}{r}\right)v_r + \mu^r, \tag{4.22}$$

differentiation of Eq. (4.20) leads to

$$\begin{aligned} \frac{d}{d\tau}v_{uS} = \Big(&2h\frac{dh}{d\tau}rv_r + 2v_r^3 Mr\mu^r - 2h^2 v_r\mu^r \\ &+E_1(r^3 v_r^2 - r^3 - 2Mr^2 v_r^2 - h^2 r)\Big)\frac{1}{2r^3 v_r^2}. \end{aligned} \tag{4.23}$$

There is an option in the code to evolve v_{uS} by Eq. (4.23). In this case, we extract v_r from the value of v_{uS}. This is done by rewriting Eq. (4.20) as a quadratic in v_r. We find

$$v_r = \frac{v_{uS} \pm \sqrt{v_{uS}^2 - \left(1 - \frac{2M}{r}\right)\left(1 + \frac{h^2}{r^2}\right)}}{\left(1 - \frac{2M}{r}\right)}. \tag{4.24}$$

When the code is evolving v_{uS} by Eq. (4.23), at each time step it also evolves v_r in the usual way. The $\pm$ in Eq. (4.24) is chosen so that the result for v_r is closest to the directly evolved value; further, if the square root in Eq. (4.24) is less than some threshold, or imaginary, the directly evolved value of v_r is not corrected. For a circular orbit of the Schwarzschild background, the square root is exactly zero, and therefore it is difficult to use this option when evolving a circular orbit.

E. The metric variable W

The only Bondi-Sachs metric variable that is non-zero in the background metric is W, and in order to improve numerical accuracy, the code treats W as the sum of the background analytic part ($W_{\rm an}$) plus a correction ($W_{\rm num}$). The values of $W_{\rm an}$ and its derivatives are found exactly, and finite differencing is applied only to the part $W_{\rm num}$. In effect, this also applies to the other metric variables, because their background analytic parts are zero.

V. COMPUTATIONAL TESTS AND RESULTS

A. Convergence

1. Initial accelerations

Firstly, we investigated the convergence of various accelerations on the initial null cone, and in so doing

tested the gravitational hypersurface equations, the gravitational evolution equation and the particle evolution equations. The tests were made with the particle initialized at $r = 9$ at the north pole with $v^r = v^p = 0$ and v^q set to the value for a circular orbit. The particle mass was $m = 10^{-4}$. The particle velocity was updated directly, without incorporating approximate conservation laws. The overlap between north and south patches was minimal ($q_s = 1.0$). The size of the polytrope was $R_* = 5.0$. The following quantities, all of which are rates of change, were determined on the initial null cone: $||J_{,u}||_\infty$, $h_{,u}$ $v_{u,u}$, $v_{r,\tau}$ and $v_{q,\tau}$. The quantities involving $u-$derivatives were found by evolving the code for one time-step and then applying the formula $Q_{,u} = (Q_1 - Q_0)/\Delta u$; the quantities involving $\tau-$derivatives are found directly by the code using data only on the initial null cone.

The following grids were used: (a) coarse, $n_x = 41$, $n_q = n_p = 25$; (b) medium $n_x = 81$, $n_q = n_p = 45$; and (c) fine, $n_x = 161$, $n_q = n_p = 85$. In the different grids, Δ_x and $\Delta_q = \Delta_p$ scale as 4:2:1. The (single) time-step was $\Delta u = 10^{-5}$, which, for all grids, is much smaller than the spatial discretization, so that second order spatial accuracy is expected. Assuming that a quantity Q behaves as $Q = a + b\Delta^n$, it is straightforward to show that

$$n = \log_2 \frac{Q_c - Q_m}{Q_m - Q_f} \tag{5.1}$$

where Q_c, Q_m and Q_f refer to the computed values of Q using the coarse, medium and fine grids, respectively.

Our results are stated in Table I: it is clear that, on the initial null cone, the polytropic model is convergent with the order n in the range 1.59 to 2.28.

2. Circular orbit

Secondly, we performed a convergence test for a particle in a circular orbit around a black hole. For the coarse and medium grids, the particle completed a whole orbit, but for the fine grid this was not possible. The particle was initialized at $r = 9$, $q = 0$ and $p = 1$ with $v^r = v^p = 0$ and v^q set to the value required for a circular equatorial orbit. The mass of the particle was $m = 10^{-6}$ and the size was $R_* = 3$ (the requirement that the polytrope should be resolvable by all grids places a lower limit on R_*). We used the technique in Sec. IV D to model approximate conservation of angular momentum, but not of energy. The angular grid-patch overlap was $q_s = 1.2$. The test results are for the time interval $0 \le u \le 20$ representing just under 1/8 of a whole orbit. The grids used were (a) coarse, $n_x = 61$, $n_q = n_p = 20$ with $du = 1.6666 \times 10^{-2}$; (b) medium, $n_x = 121$, $n_q = n_p = 35$, $du = 8.3333 \times 10^{-3}$; and (c) fine, $n_x = 241$, $n_q = n_p = 65$, with $du = 4.1666 \times 10^{-3}$.

TABLE I: Convergence of the Polytropic model

	Coarse	Medium	Fine	n
$\|\|J_{,u}\|\|_\infty$	0.4346×10^{-2}	0.4441×10^{-2}	0.4460×10^{-2}	2.28
$h_{,u}$	-0.7377×10^{-2}	-0.3436×10^{-2}	-0.2129×10^{-2}	1.59
$v_{u,u}$	0.2732×10^{-4}	0.1273×10^{-4}	0.0789×10^{-4}	1.59
$v_{r,\tau}$	-0.5050×10^{-3}	-0.5455×10^{-3}	-0.5564×10^{-3}	1.9
$v_{q,\tau}$	-1.8069×10^{-3}	-0.8416×10^{-3}	-0.5215×10^{-3}	1.59

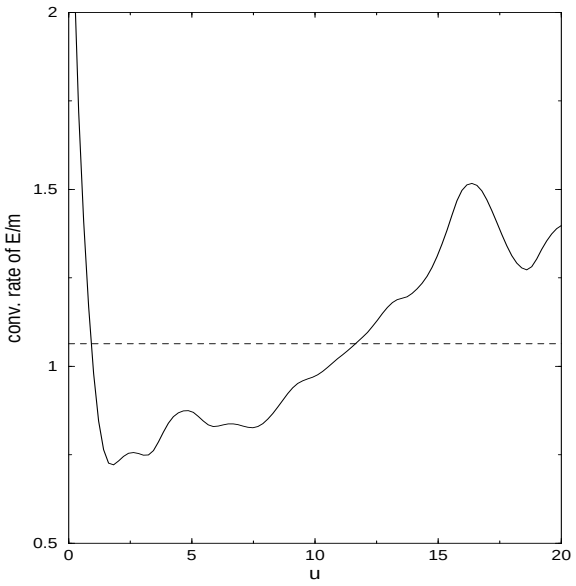


FIG. 1: Convergence rate of E/m as a function of time for $0 < u < 20$.

The convergence rate of v_u, between $u = 0$ and $u = 20$ as estimated from Eq. (5.1), is shown in Fig. 1; the average rate is $n = 1.064$, so that the effective convergence rate of the particle's energy is approximately first order. This is an artifact of the numerical scheme used in the evolution equation, which for a fixed value of the dissipation parameter is only first order in time [21].

B. Whole orbit with $m \neq 0$

The various input parameters were described in Sec. V A 2 (*circular orbit*), medium grid. The computation was run for 25,000 time steps until $u = 208$ and represents more than one orbit (which is achieved at about $u = 170$); the computation took about 24 hours of wall-clock computer time. As discussed in Sec. V A 2, the results are within the convergence regime of the numerical method. The run was performed for illustrative purposes and is not physical because a polytrope with the parameters used here would be tidally disrupted.

The results of the computation are shown in Figs. 2 to 5, in which the particle inspirals (Fig. 2), losing en-

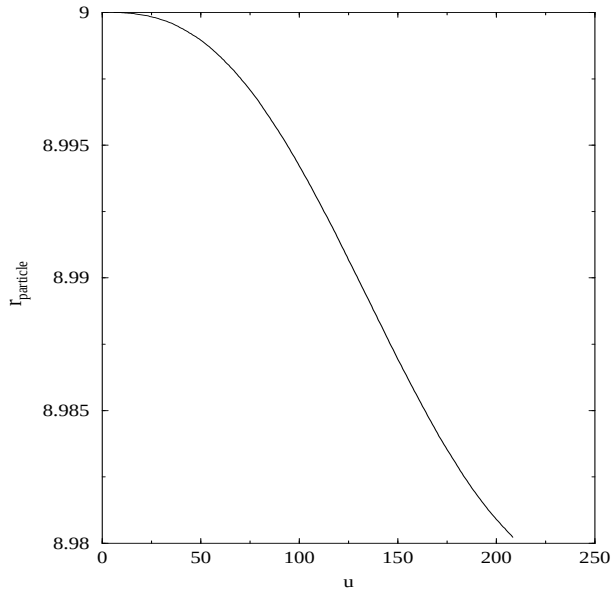


FIG. 2: r-coordinate for a complete orbit.

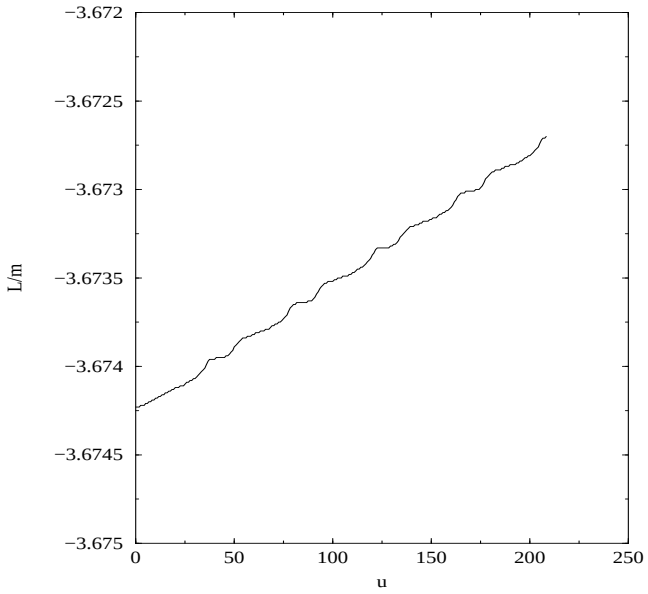


FIG. 3: Angular momentum per unit particle mass for a complete orbit.

ergy (Fig. 4) and angular momentum (Fig. 3). Figure 5 shows the time development of the L_1 norm of $J_{,u}$, which provides a measure of the dynamic activity of the gravitational field. We also performed whole orbit computations with input parameters as above, but varying the particle mass by powers of 10 in the range 10^{-4} to 10^{-9}. We found that the energy loss rate scales, as expected, as m^2.

In our numerical method, the measured inspiral was $\Delta r = -0.016$ after one complete orbit. The inspiral after one orbit is $\Delta r = -2.98 \times 10^{-6}$ according to the quadrupole formula [36], and $\Delta r = -4.75 \times 10^{-6}$ according to a perturbative method [11, 37]. The rate of energy loss, i.e. the rate of change of $E = mv_u$, is a better measure of the inspiral rate – because Δr after one orbit includes a contribution due to the orbit becoming slightly elliptical. Averaged over a complete orbit, the measured rate for the numerical method is $dE/du = 2.669 \times 10^{-13}$, whereas the quadrupole formula predicts $dE/du = 1.10 \times 10^{-16}$, and the perturbative method gives $dE/du = 1.75 \times 10^{-16}$. There is thus a discrepancy between the energy loss rates found here and by other methods. The cause of the discrepancy is not known, and may comprise a number of factors: (a) in order to resolve the particle properly, we are forced to make its size too large for it to be physical, and thus the model ignores internal tidal stresses that in this case are large (see Sec. III A); (b) lack of resolution; and (c) other. The issue is discussed further in the Conclusion, Sec. VI.

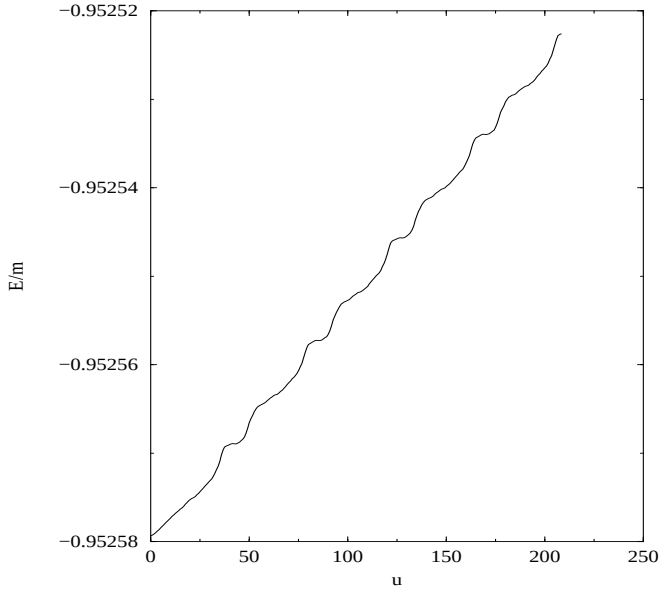


FIG. 4: Energy per unit particle mass for a complete orbit.

C. Capture of particle by the black hole

The purpose of the test was to see how the code behaves as the particle approaches the event horizon at $r = 2$, and the particle was initialized at $r = 6$, i.e. at the ISCO. The size of the particle was $R_* = 2$, and so, as

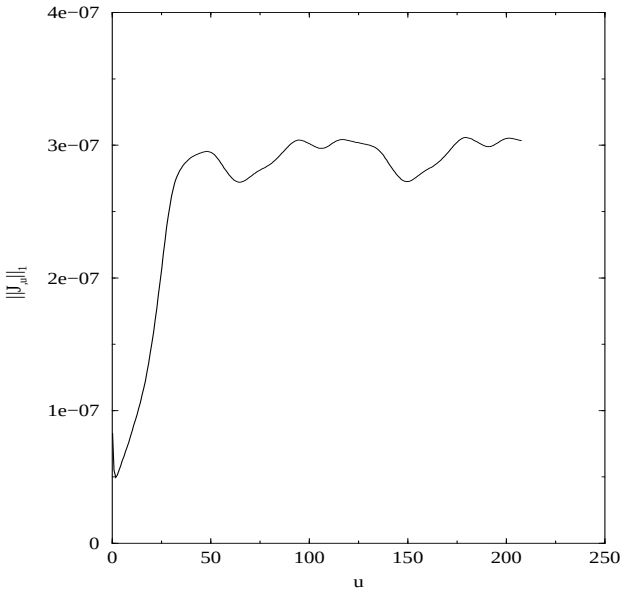


FIG. 5: L_1 norm of the radiation indicator, $\| J_{,u} \|_1$, for a complete orbit.

with the complete orbit computation, the model ignores significant tidal stresses and is not physical. In order to shorten the inspiral time the particle was given a small inward radial velocity ($v^r = -0.01$), and the angular velocity was set to that for a circular orbit in the test particle limit ($v^q = 0.0962$, $v^p = 0$). The test was performed with two different grids, enabling us to see at which stage numerical errors become significant. The grids used were $n_x = 121$, $n_q = n_p = 35$, $du = 8.3333 \times 10^{-3}$ (medium grid); and $n_x = 81$, $n_q = n_p = 25$, $du = 1.25 \times 10^{-2}$ (coarser grid).

In the coordinates being used, as $r \to 2$ the evolution variable $v_r \to \infty$. Thus, because of this coordinate effect, we expect the code to crash at some value of r just greater than 2. The results of the computation are shown in Figs. 6 to 9. In the medium grid computation, the particle inspirals until the code crashes at $u = 182.5$ with the particle at $r = 2.00077$ and $|v_r| \approx 5,000$. The particle completed just over two complete revolutions, i.e. its angular position changed by just over 4π radians during the evolution. The particle crossed $r = 2.1$ at $u = 162.5$, $r = 2.01$ at $u = 172.5$ and $r = 2.001$ at $u = 181.7$; thus demonstrating a freezing of radial position, as expected due to the redshift inherent in the u-coordinate. Throughout the computation, the position of the particle varies smoothly (Fig. 6). The particle loses energy (Fig. 8) and angular momentum (Fig. 7) at a fairly constant rate, until about $u = 150$, $r = 3.2$. Further, the activity of the gravitational field (as measured by $\| J_{,u} \|$, Fig. 9) starts to grow rapidly at this time. We have not analyzed the cause of this effect. The results of the coarser grid match those of the medium grid reasonably well until about $u = 170$, at which stage $r \approx 2.02$.

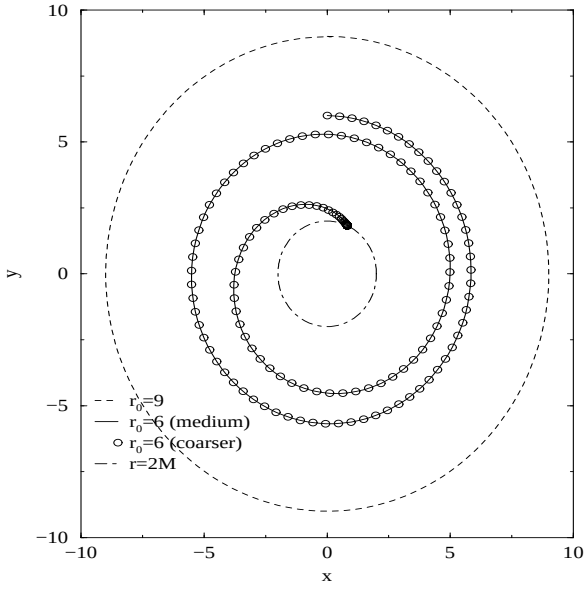


FIG. 6: The orbit, in the $(x, y) = (r\cos\phi, r\sin\phi)$ plane, traced by a particle, initially at $r = 6$, as it is captured by a black hole. Overlaid in the figure is the orbit traced by a particle initially at $r = 9$ (dotted line). The central circle indicates the location of the horizon ($r = 2$).

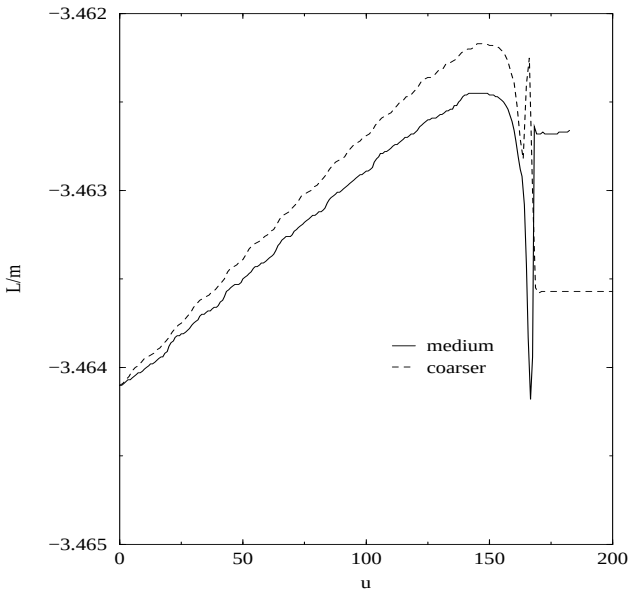


FIG. 7: Angular momentum per unit particle mass for the capture of a particle by a black hole.

D. Other experiments and computational issues

A run was performed using the same input parameters as in Sec. V B, except that $m = 0$. The orbit was found to be exactly circular, with no loss of energy or angular momentum. Because the numerical method implements the approximate conservation of angular momentum, which in this case is exact, the angular momentum behaved as expected. However, conservation of energy was not enforced. The only (minor) error was in the time for an orbit: the numerical method yielded $\Delta u = 169.638$ (for the grid used in this specific run), whereas the analytic value is $2\pi r^{\frac{3}{2}} = 169.646$. In order to check that the exact conservation of energy was not just a consequence of the orbit being exactly circular, we also did a run for a non-circular orbit, starting at $r = 9$, $q = 0$, $p = 1$ and with initial velocity $v^r = 0$, $v^q = 0.047$, $v^p = 0$. The particle was found to move in an orbit between $r = 9$ and $r = 11.79$, and there was a very small change in v_u: energy was conserved, in the sense of $dv_u/du = 0$, to the order of one part in 10^{14}.

A simple test of the code is to determine if it produces results concerning caustic formation that are consistent with the estimate given in Eq. (3.10). We performed a number of short runs (up to 100 iterations), each with a different value of particle mass m, and made a binary chop search to find the critical value of m above which the code crashes due to the onset of caustic formation (indicated by the metric variable $\beta \to \infty$ at $\mathcal{I}^+$). The test was performed with initial velocity $v^i = 0$, initial position $r = 9$ at the north pole, and polytropic radius $R_* = 2$.

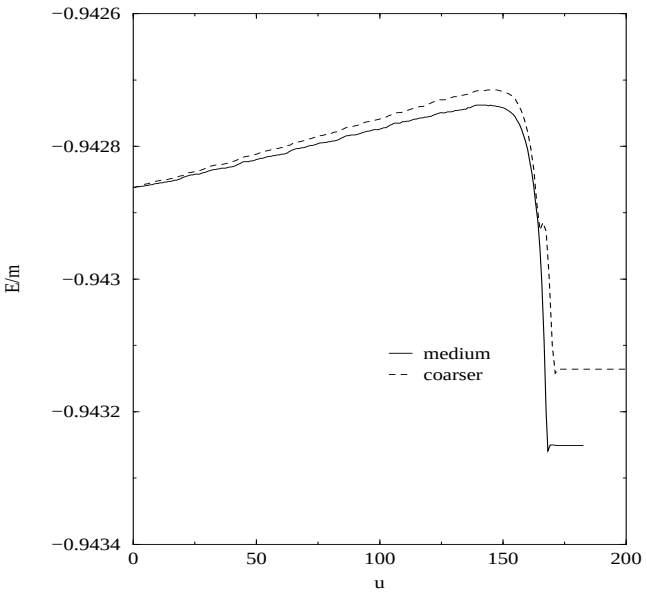


FIG. 8: Energy per unit particle mass for the capture of a particle by a black hole.

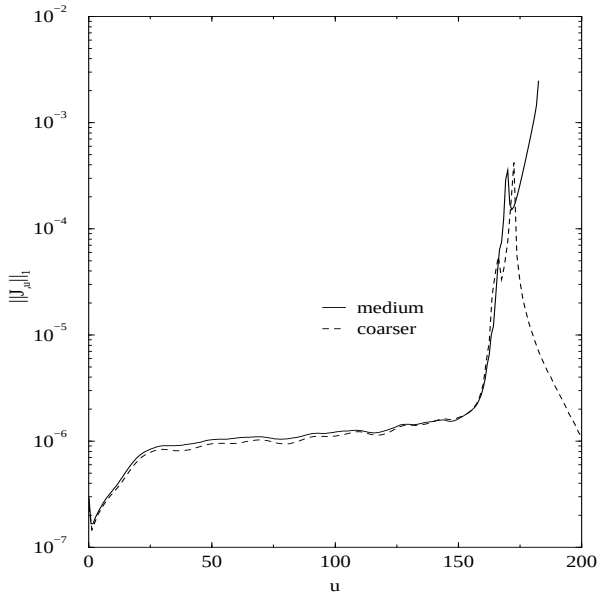


FIG. 9: L_1 norm of the radiation indicator, $\| J_{,u} \|_1$, shown using a logarithmic scale in the vertical axis, for the capture of a particle by a black hole.

The grid discretization was $n_x = 121$, $n_q = n_p = 35$, with time step $dt = 8.3333 \times 10^{-3}$. We found that the code behaved properly with $m = 0.03$ but crashed when $m = 0.04$, consistent with the critical value of $m = 0.111$ indicated by Eq. (3.10).

Unfortunately, it is not possible, at this time, to present results on gravitational radiation output. The module used in the code for calculating the news [21] was originally developed and tested under conditions in which the fields are well resolved at $\mathcal{I}^+$, which is not the case for particle applications. Improvements in the news computation have recently been investigated [38, 39], but it is not yet known whether the radiation from a particle source can be reliably computed. Results will be reported elsewhere after the necessary development and testing.

The tests were performed on a Linux machine with a single processor running at 1.8GHz. The complete orbit run reported in Sec. V B used a grid of 121×35^2 points (on each angular patch) and 25,000 time steps. The run time was about 24 hours. Of course, the run time scales with grid discretization as Δ^{-4}.

VI. CONCLUSION

In this paper we have described and implemented the PP method for evolving the full Einstein equations using a characteristic evolution code. The method could be adapted and used within other numerical relativity frameworks. The PP method can be a useful tool in

modeling astrophysical situations involving a black hole and another much smaller object, in a regime in which a full hydrodynamic model is not necessary. We have demonstrated that the method works in the sense that it computes orbits that are convergent, and deviations from a Schwarzschild orbit scale as expected with particle mass m. However, the computed inspiral rate was much larger than that predicted by other methods. A feature of the code is that it avoids the computational expense of modeling the material object by means of relativistic hydrodynamics.

The PP method has the potential to supply accurate orbits, including inspirals towards the ISCO and plunges to the black hole, as well as the associated gravitational radiation output. Such results would be useful both directly, and also indirectly in providing error bars against which other methods could be tested. In the tests described here, the need to resolve the particle has prevented us from making the particle radius small enough so that its local rigidity is justified. In order to achieve a proper physical basis for the model, we envisage the following future work

1. It is necessary to investigate the effect of the polytrope radius (R_*) on particle motion. On physical grounds, one would expect that in some regime the particle motion should be independent of R_*. (Of course, taking the limit $R_* \to 0$ is equivalent to changing from the polytropic to a $\delta-$function model, and this link provided motivation for the investigation of that model).

2. Once parameters for the model that are physically realistic can be attained, it will be necessary to investigate whether the PP method computes reliable energy loss rates.

3. The gravitational radiation output (Bondi news function) is required, both to supply a waveform and to check the energy balance (the rate of loss of orbital energy mv_u should be of the same magnitude as the radiation power).

4. Once the above issues have been resolved, it will be necessary to validate the PP method by obtaining results that agree, in some regime, with results obtained by another method.

Acknowledgments

We thank Manuela Campanelli and Carlos Lousto for discussions, and Scott Hughes for providing information on perturbative results. We benefited from the hospitality of the Max-Planck-Institut für GravitationsPhysik, Albert-Einstein-Institut, the Center for Gravitational Wave Physics at Pennsylvania State University, and the Kavli Institute for Theoretical Physics at the University of California at Santa Barbara. This work was partially supported by the National Research Foundation, South Africa under Grant number 2053724, and by NSF Grants PHY-9988663 to the University of Pittsburgh and PHY-0135390 to Carnegie Mellon University, and by NSF Grants PHY-0114375 to the Pennsylvania State University, and PHY-9907949 to the University of California at Santa Barbara.

APPENDIX A: THE GEODESIC EQUATION

We have used Maple to compute the form of Eq. (4.1) for the metric (2.1). The angular part of v_i, v_A is represented by the spin weighted quantity $V_{ang} = v_A q^A$. Further, for ease of application to the approximate conservation method (Secs. III C and IV D), the formulas are presented with the zeroth order quantities (in each case, the first line) shown separately from the perturbative (E_i) quantities.

$$
\begin{aligned}
\frac{dv_r}{d\tau} &= \frac{2\bar{V}_{ang}V_{ang} - v_r^2(rW_{,r} - W)r}{2r^3} \\
&+ \Big(+ 4\bar{V}_{ang}V_{ang}(1-K) - 2(e^{-2\beta}-1)v_r^2(rW_{,r}-W)rK - 2J\bar{V}_{ang}^2K + 4\bar{V}_{ang}V_{ang}\bar{J}J - r\bar{V}_{ang}V_{ang}J_{,r}\bar{J} \\
&- r\bar{V}_{ang}V_{ang}J\bar{J}_{,r} - 4\beta_{,r}e^{-2\beta}v_r r^3\bar{U}V_{ang}K - 4\beta_{,r}e^{-2\beta}v_r r^3U\bar{V}_{ang}K - 2\bar{J}V_{ang}^2K \\
&+ 4e^{-2\beta}v_r^2\beta_{,r}(r+W)r^2K - 8\beta_{,r}e^{-2\beta}v_r r^3v_uK + rJ_{,r}\bar{V}_{ang}^2K + 2e^{-2\beta}v_r r^3\bar{U}_{,r}V_{ang}K \\
&+ 2e^{-2\beta}v_r r^3U_{,r}\bar{V}_{ang}K + r\bar{J}_{,r}V_{ang}^2K\Big)\frac{1}{4Kr^3}; \qquad \text{(A1)} \\
\frac{dV_{ang}}{d\tau} &= -\frac{(q+ip)\bar{V}_{ang}V_{ang}}{r^2}
\end{aligned}
$$

$$
\begin{aligned}
&+ \Big(-4(q+ip)\bar{V}_{ang}V_{ang}(K-1) + 4(\eth K)J\bar{J}\bar{V}_{ang}V_{ang} - 2(\eth J)K\bar{J}\bar{V}_{ang}V_{ang} - 2(\eth \bar{J})KJ\bar{V}_{ang}V_{ang} \\
&- 4e^{-2\beta}v_r(\eth\beta)r^2U\bar{V}_{ang} - 4e^{-2\beta}v_r(\eth\beta)r^2\bar{U}V_{ang} - 2e^{-2\beta}v_r^2(\eth W)r + 4e^{-2\beta}v_r^2(r+W)(\eth\beta)r \\
&- 8e^{-2\beta}v_r(\eth\beta)r^2v_u + (\eth\bar{J})J^2\bar{V}^2_{ang} + (\eth J)\bar{J}^2V^2_{ang} - 2(\eth K)JK\bar{V}^2_{ang} - 2(\eth K)\bar{J}KV^2_{ang} + 2(\eth K)\bar{V}_{ang}V_{ang} \\
&+ (\eth J)\bar{V}^2_{ang}\bar{J}J + (\eth\bar{J})V^2_{ang}\bar{J}J + 4ip\bar{J}V^2_{ang} + (\eth J)\bar{V}^2_{ang} + (\eth\bar{J})V^2_{ang} + 4q\bar{J}V^2_{ang} + 2r^2e^{-2\beta}v_r(\eth\bar{U})V_{ang} \\
&+ 2r^2e^{-2\beta}v_r(\eth U)\bar{V}_{ang} + 4r^2e^{-2\beta}v_rq\bar{U}V_{ang} + 4ir^2e^{-2\beta}v_rp\bar{U}V_{ang}\Big)\frac{1}{4r^2}. \qquad \text{(A2)}
\end{aligned}
$$

[1] Y. Mino, Phys. Rev. D **67**, 084027 (2003).
[2] L. Barack and A. Ori, Phys. Rev. Lett. **90**, 111101 (2003).
[3] L. Blanchet, G. Faye, B. R. Iyer, and B. Joguet, Phys. Rev. D **65**, 061501 (2002).
[4] L. Gualtieri, E. Berti, J. A. Pons, G. Miniutti, and V. Ferrari, Phys. Rev. D **64**, 104007 (2001).
[5] L. Barack, Y. Mino, H. Nakano, A. Ori, and M. Sasaki, Phys. Rev. Lett. **88**, 091101 (2002).
[6] M. J. Pfenning and E. Poisson, Phys. Rev. D **65**, 084001 (2002).
[7] L. Barack and C. O. Lousto, Phys. Rev. D **66**, 061502 (2002).
[8] C. O. Lousto, Class. Quant. Grav. **18**, 3989 (2001).
[9] T. C. Quinn and R. M. Wald, Phys. Rev. D **56**, 3381 (1997).
[10] Y. Mino, M. Sasaki, and T. Tanaka, Prog. Theor. Phys. Suppl. **128**, 373 (1997).
[11] K. Glampedakis, S. A. Hughes, and D. Kennefick, Phys. Rev. D **66**, 064005 (2002).
[12] L. M. Burko, Phys. Rev. D **67**, 084001 (2003).
[13] J. Font, T. Goodale, S. Iyer, M. M. L. Rezzolla, E. Seidel, N. Stergioulas, W. Suen, and M. Tobias, Phys. Rev. D **65**, 084024 (2002).
[14] M. Shibata and K. Uryu, Phys. Rev. D **64**, 104017 (2001).
[15] E. Gourgoulhon, P. Grandclment, K. Taniguchi, J.-A. Marck, and S. Bonazzola, Phys. Rev. D **63**, 064029 (2001).
[16] J. A. Faber and F. A. Rasio, Phys. Rev. D **63**, 044012 (2001).
[17] K. Oohara and T. Nakamura, Prog. Theor. Phys. **136**, 270 (1999).
[18] P. Papadopoulos and J. A. Font, Phys. Rev. D **61**, 024015 (2000).
[19] M. Shibata and K. Uryu, in *Proceedings of the 16th International Conference on General Relativity & Gravitation*, edited by N. T. Bishop and S. D. Maharaj (World Scientific, Singapore, 2002).
[20] L. S. Finn and K. S. Thorne, Phys. Rev. D **62**, 124021 (2000).
[21] N. T. Bishop, R. Gómez, L. Lehner, M. Maharaj, and J. Winicour, Phys. Rev. D **56**, 6298 (1997).
[22] R. Gómez, Phys. Rev. D **64**, 024007 (2001).
[23] R. A. Isaacson, J. S. Welling, and J. Winicour, J. Math. Phys. **26**, 2859 (1985).
[24] N. T. Bishop, R. Gómez, L. Lehner, and J. Winicour, Phys. Rev. D **54**, 6153 (1996).
[25] N. T. Bishop, Class. Quantum Grav. **10**, 333 (1993).
[26] N. T. Bishop, C. J. S. Clarke, and R. A. d'Inverno, Class. Quantum Grav. **7**, L23 (1993).
[27] R. A. Isaacson, J. S. Welling, and J. Winicour, J. Math. Phys. **24**, 1824 (1983).
[28] H. Bondi, M. J. G. van der Burg, and A. W. K. Metzner, Proc. R. Soc. London **A269**, 21 (1962).
[29] L. A. Tamburino and J. Winicour, Phys. Rev. **150**, 1039 (1966).
[30] R. K. Sachs, Proc. R. Soc. London **A270**, 103 (1962).
[31] R. Gómez, L. Lehner, P. Papadopoulos, and J. Winicour, Class. Quantum Grav. **14**, 977 (1997).
[32] N. T. Bishop, R. Gómez, L. Lehner, M. Maharaj, and J. Winicour, Phys. Rev. D **60**, 024005 (1999).
[33] S. Chandrasekhar, *An introduction to the study of stellar structure* (Dover, New York, 1967).
[34] J. Winicour, J. Math. Phys. **24**, 1193 (1983).
[35] J. Winicour, J. Math. Phys. **24**, 2056 (1983).
[36] C. W. Misner, K. S. Thorne, and J. A. Wheeler, *Gravitation* (Freeman, San Francisco, 1973).
[37] S. A. Hughes, Phys. Rev. D **61**, 084004 (2000).
[38] Y. E. Zlochower, Ph.D. thesis, University of Pittsburgh (2002).
[39] N. T. Bishop and S. S. Deshingkar, Phys. Rev. D **68**, 024031 (2003).